Research Report

Practical Upper Limits of Conversion Efficiency of Solar Cells Utilizing Hot-Carrier Energies

Yasuhiko Takeda and Tomoyoshi Motohiro

Report received on Jul. 16, 2012

ABSTRACT We have constructed new detailed-balance models to calculate limiting conversion efficiencies of two major types of third-generation solar cells: multiple exciton generation (MEG) solar cells and hot-carrier solar cells (HC-SCs), which have attracted increasing attention due to their potentially high conversion efficiencies over 50%. These models enable evaluation of the detrimental effects of energy dissipation processes in these solar cells that could be eliminated in principle, but are unavoidable in practice. Quantum dots (QDs) of PbSe and Si have been most intensively investigated as candidate materials for MEG solar cells, in which multiple excitons or carriers are generated per single absorbed photon but have not been found to be promising. Although InAs fulfills the material selection criteria for efficient MEG, experimentally observed quantum yields of photon-to-carrier conversion are considerably lower than that required for high conversion efficiency. In HC-SCs, photogenerated carrier energy in excess of the bandgaps can be converted to electricity by extracting the high-energy carriers (hot carriers) before they are completely thermalized, i.e., before the excess carrier energy dissipates to phonons. Although the phonon-bottleneck effect in QDs can suppress thermalization, the effect demonstrated for InAs QDs is not sufficient. Thus, it seems very difficult for these types of solar cells to compete against existing single-junction solar cells such as Si and $CuIn_{1-x}Ga_xSe$ (CIGS) cells for rooftop use and triple-junction solar cells using III-V compound semiconductors coupled with solar concentrators.

KEYWORDS Solar Cells, Multiple Exciton Generation, Carrier Multiplication, Hot Carriers, Limiting Efficiency, Detailed Balance, Quantum Dots

1. Introduction

In a conventional solar cell, a photon with an energy higher than the bandgap of the light-absorbing material used in the cell is absorbed to generate a carrier with an energy equal to the photon energy. However, carrier energy in excess of the bandgap of the absorber is immediately transferred to phonons, which temperature equals the room temperature, i.e., thermalization of carriers occur within several picoseconds in most cases. Therefore, the excess carrier energy cannot be converted to electricity. This thermalization is one of the most significant energy dissipation channels in the photovoltaic conversion process.[1] The limiting conversion efficiency of single-junction solar cells (1J-SCs), i.e., the Shockley-Queisser (S-Q) limit, is determined assuming that (i) the absorber has a single bandgap, (ii) one absorbed photon generates one carrier, and (iii) the photogenerated carriers are extracted after being completely thermalized.[2]

Figure 1 summarizes the previously proposed concepts to exceed the S-Q limit. The most straightforward method based on existing technologies is the use of plural absorbers with different bandgaps for spectral splitting to reduce the excess carrier energies. In fact, triple-junction solar cells (3J-SCs)

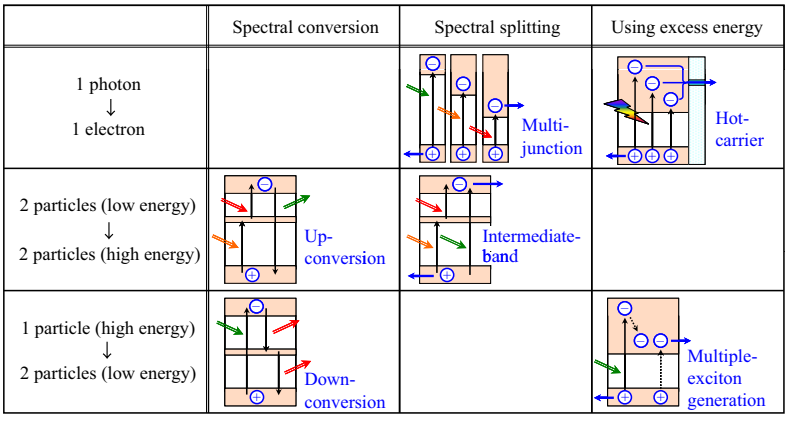

Fig. 1 Types of solar cells to exceed the Shockley-Queisser (S-Q) limit.

using III-V compound semiconductors have successfully realized conversion efficiencies over 40% under concentrated solar irradiation,[3,4] which are significantly higher than the best record of 1J-SCs using GaAs (29%).[3] 4-junction solar cells using new materials have been intensively investigated with an aim to further increase the efficiency toward 50%.[5,6] However, the complicated multilayered structures required for 3J-SCs (and for 4-junction cells) raise the costs, and therefore 3J-SCs are currently used only for solar-concentrator systems that employ Fresnel lenses and concave mirrors to reduce the proportion of cell to module area, and for space applications.

Third-generation solar cells attempt to achieve very high efficiency over 50% with only a small increase in areal costs compared with those of conventional 1J-SCs. Among them, the idea to achieve spectral splitting using only one absorber has been implemented with an intermediate-band solar cell (IB-SC) that uses an absorber with an intermediate band (IB) in its fundamental bandgap.[7,8] In an IB-SC, low energy photons excite electrons from the valence band (VB) to the IB and then from the IB to the conduction band (CB), i.e., two low-energy particles generate one high-energy particle, similar to an up-converter.[9] The two-step excitation via the IB has been demonstrated using highly mismatched semiconductor alloys such as ZnTe:O[10] and GaAs:N,[11] and InAs QDs embedded in GaAs-related matrices.[12,13] However, the current R&D status remains at the proof-of-concept stage, and improvement in the conversion efficiency has not yet been realized compared with that of 1J-SCs.

On the other hand, hot-carrier solar cells (HC-SCs) and solar cells utilizing multiple exciton generation (MEG) aim to convert the excess carrier energies to electricity. In an MEG cell, a high-energy photon generates two or more carriers, which results in a larger output current density than that of a 1J-SC with the same bandgap.[14-16] This process is similar to that in a down-converter,[17] because one high-energy particle is converted to two (or more) low-energy particles. In contrast, high energy carriers are directly extracted in an HC-SC, which contributes to a higher output voltage.[18,19]

To date, detailed-balance calculations have been carried out on MEG solar cells and HC-SCs to determine the limiting conversion efficiency, but only under the ideal conditions. In the present study, we construct new detailed-balance models including detrimental factors that could be eliminated in principle, but are unavoidable in practice, i.e., energy dissipation processes of photogenerated carriers, to evaluate the practical upper limits of conversion efficiency of these cells. We first deal with MEG solar cells in Sec. 2, and then HC-SCs in Sec. 3. In Sec. 4, we summarize the results and present concluding remarks.

2. Multiple Exciton Generation (MEG) Solar Cells

The S-Q limit is derived assuming that the quantum yield of photon-to-carrier conversion, γ, equals unity at photon energies higher than the bandgap of the absorber, as mentioned in Introduction. From an energy conservation perspective, when a photon which energy is higher than twice the bandgap is absorbed, two carriers (and three carriers for a photon with an energy three times higher than the bandgap) can be generated. Such phenomena, often referred to as MEG, have recently been demonstrated in semiconductor quantum dots (QDs) of a wide variety of materials, including PbS,[20,21] PbSe,[21-23] PbTe,[24] CdSe,[25] CdTe,[26] InAs,[27,28] InP,[29] and Si.[30] However, there are considerable variations in the reported γ values,[16,22,23] depending on surface treatments of the QDs and/or experimental details. Therefore, it is still under debate whether MEG occurs more efficiently in QDs than in bulk materials.[22,23,31]

Three solar-cell configurations have been proposed to utilize MEG in QDs:[32] (a) QD arrays as the *i* region of a *p*-*i*-*n* junction, (b) QDs as sensitizers coupled with a wide-bandgap semiconductor (analogous to dye-sensitized solar cells), and (c) QDs dispersed in a blend of electron- and hole-conducting polymers. Promising results for the extraction of multiply generated carriers, i.e., ratios of current density to absorbed photon flux density (internal quantum yield) higher than unity, have been demonstrated using the configuration (a).[14,15]

In the following, we evaluate the effect of the γ characteristics in detail with respect to the effective masses of electrons and holes in the QD materials and the potential-barrier height for photogenerated carriers in the QDs.[33,34] The influence of solar irradiation intensity up to 1000 sun, which is approximately the practical upper limit,[35,36] is also investigated.

2. 1 Detailed-balance Including MEG

The absorber used in an MEG solar cell is assumed

to comprise QDs embedded in a barrier material, which is consistent with the configuration (a) mentioned above, i.e., QD arrays as the *i* region of a *p-i-n* junction. Energy diagrams of the absorbers and their MEG processes are schematically illustrated in **Fig. 2**.

The conversion efficiency of a solar cell utilizing MEG is derived using the detailed-balance model.[37] The output current density, J_{out}, is determined from the difference between the absorbed and emitted photon fluxes, J_{abs} and J_{em}, respectively:

$$J_{out} = \int_{\varepsilon_g}^{\infty} d(\hbar\omega)\left(\gamma(\hbar\omega)\, j_{sun}(\hbar\omega) - j_{em}(\hbar\omega)\right) = J_{abs} - J_{em}, \quad \cdots\cdots\cdots\cdots (1)$$

where $j_{sun}(\hbar\omega)$ and $j_{em}(\hbar\omega)$ are the solar spectral photon flux and the emitted photon flux, respectively, ε_g the energy gap of the QDs, $\hbar$ the Dirac constant, and ω the frequency of light. Nonradiative recombination processes including Auger recombination are neglected. The quantum yield of photon-to-carrier conversion as a function of $\hbar\omega$, $\gamma(\hbar\omega)$, equals unity at around ε_g, because photons with an energy $\hbar\omega$ higher than ε_g are assumed to be completely absorbed. When MEG occurs at a large $\hbar\omega$, $\gamma(\hbar\omega)$ exceeds unity. When $\hbar\omega$ is sufficiently large, it is possible that more than two carriers are generated by a single absorbed photon, and thus $\gamma(\hbar\omega)$ has a value higher than two.

When MEG occurs, the reverse process can also take place, i.e., multiple carriers can generate a single high-energy photon during the emission process. In this process, the carrier energy represented by the product of $\gamma(\hbar\omega)$ and the quasi-Fermi level splitting between the CB and VB, $\Delta\mu$, is converted to the photon energy of $\hbar\omega$, with the Carnot efficiency:[38,39]

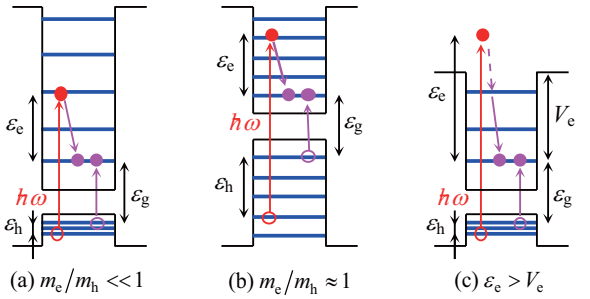

Fig. 2 Schematic energy diagrams and excitation, energy dissipation and MEG processes in QDs surrounded by barrier materials.

$$\hbar\omega\left(1 - \frac{T_{RT}}{T_{rad}}\right) = \gamma(\hbar\omega)\,\Delta\mu\,, \quad \cdots\cdots\cdots\cdots (2)$$

where T_{RT} and T_{rad} are the room temperature and radiation temperature, respectively. Using this relationship, the Planck's law at a radiation temperature T_{RT} can be generalized to:

$$j_{em}(\hbar\omega) = \frac{2\pi}{h^3 c^2} \frac{\gamma(\hbar\omega)(\hbar\omega)^2}{\exp\left[\left(\hbar\omega - \gamma(\hbar\omega)\,\Delta\mu\right)/k_B T_{RT}\right] - 1}, \quad \cdots\cdots\cdots\cdots (3)$$

where c denotes the velocity of light in vacuum, k_B the Boltzmann constant, and h the Planck constant. When $\gamma(\hbar\omega)$ equals unity over the entire energy range, Eq. (1) is identical to the standard detailed-balance formulation for conventional 1J-SCs, and gives the same results as the S-Q formulation.[2]

The output voltage, V_{out}, is identical to $\Delta\mu$. Thus the output power, P_{out}, equals the product of J_{out} and $\Delta\mu$, and the conversion efficiency, η, is the ratio of P_{out} to the incident energy flux:

$$P_{out} = J_{out}\,\Delta\mu\,, \quad \cdots\cdots\cdots\cdots (4)$$

$$\eta = P_{out} \Big/ \int_0^{\infty} d(\hbar\omega)\,\hbar\omega\, j_{abs}(\hbar\omega)\,. \quad \cdots\cdots\cdots\cdots (5)$$

For numerical evaluations in the next subsection, the AM1.5G spectrum was used up to 10 sun solar irradiation intensity, and the AM1.5D spectrum was used for higher intensity with consideration for the use of tracking solar concentrators.[40]

2. 2 Effects of MEG Quantum Yield Features

We investigated three characteristics of $\gamma(\hbar\omega)$: the threshold photon energy above which it is higher than unity, its upper limit, and the steepness of its increase at around the threshold photon energies.

2. 2. 1 Threshold Photon Energy of MEG Quantum Yields

The threshold of photon energy above which MEG can occur is mainly dominated by the ratio of photogenerated electron energy to the hole energy. The

expression of electron energy derived from a parabolic two-band model with a direct bandgap in a bulk material can be approximately applied to QDs, because $\hbar\omega$ is much larger than ε_g and the energy levels involved in MEG processes measured from the band edge are sufficiently high.[25,27]

The energy of an electron measured from the first quantum-confined level of conduction electrons, ε_e, is expressed as (See Fig. 2):

$$\varepsilon_e = \frac{(\hbar\omega - \varepsilon_g)\, m_h}{m_e + m_h}, \quad \cdots\cdots (6)$$

where m_e and m_h are the effective masses of electrons in the CB and holes in the VB, respectively. When ε_e is larger than ε_g, MEG can occur using ε_e. The threshold of two-carrier generation (one additional carrier by MEG), $\hbar\omega_{th\text{-}e}(1)$, is derived as a solution of the equation $\varepsilon_e = \varepsilon_g$:

$$\hbar\omega_{th-e}(1) = \left(2 + \frac{m_e}{m_h}\right)\varepsilon_g \quad \cdots\cdots (7)$$

The hole energy ε_h, and the threshold for MEG using ε_h, $\hbar\omega_{th\text{-}h}(1)$, are similarly derived:

$$\varepsilon_h = \frac{(\hbar\omega - \varepsilon_g)\, m_e}{m_e + m_h}, \quad \cdots\cdots (8)$$

$$\hbar\omega_{th-h}(1) = \left(2 + \frac{m_h}{m_e}\right)\varepsilon_g \quad \cdots\cdots (9)$$

When $\hbar\omega$ is sufficiently large, plural carriers can be additionally generated by MEG, and the thresholds ($\hbar\omega_{th\text{-}e}(2)$, $\hbar\omega_{th\text{-}e}(3)$, …) are derived in a similar manner.

The values of $\gamma(\hbar\omega)$ with the ideal step-like increases at the thresholds are depicted in **Fig. 3**(a). When m_e/m_h is close to zero as shown in Fig. 2(a), an additional carrier is generated by MEG ($\gamma(\hbar\omega) = 2$) using ε_e at $\hbar\omega \geq 2\,\varepsilon_g$, and $\gamma(\hbar\omega) = 3$ at $\hbar\omega \geq 3\,\varepsilon_g$. For $m_e/m_h = 0.2$, the thresholds $\hbar\omega_{th\text{-}h}(1)$ and $\hbar\omega_{th\text{-}e}(2)$ equal $2.2\varepsilon_g$ and $3.4\varepsilon_g$, respectively. In these cases, ε_h is too small to generate another carrier in the calculated $\hbar\omega$ range. In contrast, $\gamma(\hbar\omega)$ increases from 1 to 3 at $\hbar\omega = 3\varepsilon_g$ when m_e/m_h equals 1, because ε_e equals ε_h, and consequently ε_e and ε_h contribute equally to MEG, see Fig. 2(b).

The relationship for $\hbar\omega_{th\text{-}e}(1)$ and $\hbar\omega_{th\text{-}h}(1)$ derived here has been experimentally confirmed to be applicable to various direct-bandgap materials, as summarized in **Table 1**, and also provides a rough estimation for Si, although Si has an indirect bandgap. As for PbSe, $\hbar\omega_{th\text{-}h}(1)$ is the lowest threshold, because m_h is smaller than m_e.

The resultant conversion efficiencies are shown in Fig. 3(b). When m_e/m_h is rather small, conversion

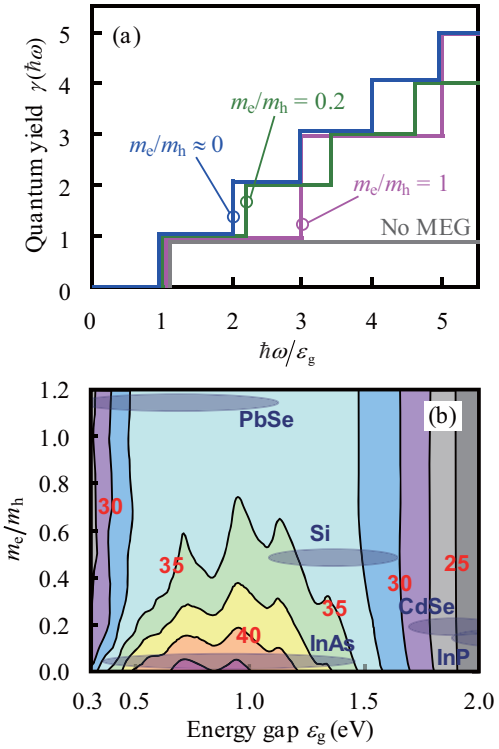

Fig. 3 (a) Model quantum yields ($\gamma(\hbar\omega)$) with different m_e/m_h values. (b) Contour plot of the conversion efficiency of MEG solar cells under 1 sun solar irradiation.

Table 1 Effective mass ratio values in bulk materials and MEG thresholds calculated using Eqs. (7) and (9), and those experimentally determined for QDs.

	m_e/m_h [a]	$\hbar\omega_{th-e}(1)/\varepsilon_g$	$\hbar\omega_{th}/\varepsilon_g$(experiment)
InAs	0.04	2.04	2.0 [b]
InP	0.18	2.18	2.1 [c]
CdSe	0.20	2.20	2.5 [d]
Si	0.48	2.48	2.4 [e]
PbSe	$m_h/m_e = 0.87$	$\hbar\omega_{th-h}(1) = 2.87$	2.5-3.0 [f]

a: Ref. 41, b: Ref. 27, c: Ref. 29, d: Ref. 25, e: Ref. 30, f: Refs. 22,23

efficiency higher than the S-Q limit (34%) can be achieved. The optimal ε_g is around 0.7-1.0 eV, which is significantly smaller than that determined from the S-Q formulation (1.4 eV), because a small ε_g widens the spectral range contributing to MEG, and as a consequence, significantly improves the short-circuit current density, which outweighs the influence of lowering the open-circuit voltage.

Another interpretation is that the lower optimal ε_g by MEG is due to suppressed dissipation of the carrier energy in excess of the energy gap. In conventional 1J-SCs, dissipation of the excess carrier energy becomes more significant with decreasing ε_g, although the total amount of absorbed energy increases. When MEG occurs, the energy dissipation is suppressed, which results in a smaller optimal ε_g.

In contrast, at a larger ε_g, the improvement by MEG is slight, because the number of photons contributing to MEG accounts for only a small fraction of the total photon number.

The most significant finding is that the conversion efficiency is drastically lowered with increasing m_e/m_h up to 1. This is due to the shift of $\hbar\omega_{th\text{-}e}(n)$ to larger energy, according to Eq. (7), etc., as shown in Figs. 2 and 3(a), and consequently the number of photons contributing to MEG decreases at a given ε_g.

This result provides a guide for selection of the QD materials. The bandgap and m_e/m_h in bulk materials are summarized in Table 1, and plotted in Fig. 3(b) with the values of ε_g for QDs used in experimental demonstrations of MEG. PbSe does not improve the conversion efficiency, because the m_e/m_h value is close to 1, although PbSe QDs were first reported to exhibit efficient MEG and have been most intensively investigated. Si QDs have also attracted much attention due to their nontoxicity and abundance, but they also show no particular promise. The large values of ε_g for InP or CdSe are not suitable, although the m_e/m_h values are rather small. Thus, among the materials listed in Table 1, only InAs fulfills the requisite of ε_g and m_e/m_h for high conversion efficiency.

2. 2. 2 Upper Limit of MEG Quantum Yield

There is, in principle, no upper limit of $\gamma(\hbar\omega)$ if the photogenerated carriers in the QDs are substantially confined by infinitely high potential barriers. However, the potential barrier height must be restricted for solar cell applications, so that carriers can be extracted from the QDs to external electrodes.

Although the origin of efficient MEG is not yet fully understood, all the mechanisms proposed require that photogenerated carriers are still confined in QDs for strong carrier-carrier interaction.[42,43] When an electron is excited beyond the potential barrier, it evidently loses its energy to rapidly reach the top of the potential barrier, followed by contribution to MEG, as shown in Fig. 2(c). Thus, the potential barrier height for electrons, V_e, determines the upper limit of $\gamma(\hbar\omega)$, which is represented as γ_{limit}.

A higher V_e allows a higher γ_{limit}, but results in more significant disturbance of the electron transport, and consequently would lower the conversion efficiency in reality. Therefore, it is necessary to find suitable values of γ_{limit} and V_e to design a concrete device structure.

Figure 4(a) shows $\gamma(\hbar\omega)$ models for different γ_{limit} values. Here, m_e/m_h equals 0.04, which is the value for InAs. In this case, ε_h is too small to be utilized for MEG under the terrestrial solar spectrum. Therefore, the potential barrier height for holes does not directly affect γ_{limit}.

The resultant conversion efficiency is shown in Fig. 4(b). A significant increase in the efficiency is achieved for $\gamma_{limit} = 2$ compared with that for no MEG

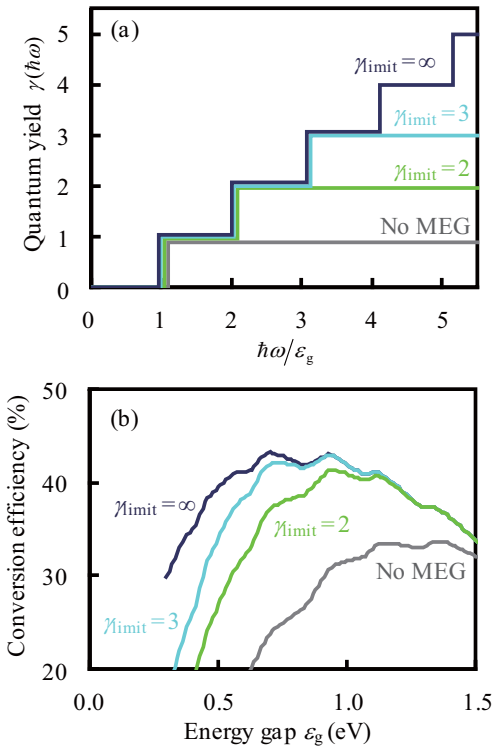

Fig. 4 (a) Model quantum yields ($\gamma(\hbar\omega)$) with different upper limits (γ_{limit}). m_e/m_h = 0.04. (b) Conversion efficiency of MEG solar cells under 1 sun solar irradiation.

over the entire ε_g range, and the gain, which is defined as the improvement in the maximal efficiency as a function of ε_g, is as high as 7% (41% at ε_g = 0.95 eV for γ_{limit} = 2 and 34% at ε_g = 1.35 eV for no MEG). The efficiency at small ε_g is further increased for γ_{limit} = 3, because a considerable number of photons contributes to three-carrier generation. However, the gain for γ_{limit} = 3 is only 2% higher (43% efficiency at ε_g = 0.95 eV) than that for γ_{limit} = 2. Even for γ_{limit} = ∞, the maximal efficiency is very close to the value for γ_{limit} = 3.

These results serve as a guide for selection of the matrix surrounding the QDs. To realize γ_{limit} = 2, a V_e slightly larger than ε_g is required. The offset of the CBs of the QDs and barriers, which is equal to the sum of V_e and the confinement energy of the lowest level in the QDs (the energy difference between the lowest confined level and the minimum level of the CB in the barriers), as shown in Fig. 2, should be around 1.5-2.0 eV. $Al_xGa_{1-x}As$ is a possible candidate for the barrier material coupled with InAs QDs. The Stranski-Krastanov growth mode can be applied to fabricate this combination. Doping with Sb enables precise control of the band offset.[44] However, for γ_{limit} = 3, another material with a larger ε_g is required.

2. 2. 3 Steepness of Increase in MEG Quantum Yield

If there were no energy dissipation from photogenerated carriers prior to MEG, then $\gamma(\hbar\omega)$ would exhibit step-like increases at $\hbar\omega_{th}(1)$, $\hbar\omega_{th}(2)$, etc., as shown in Figs. 3(a) and 4(a). However, carrier-phonon interaction competes against MEG, although it can be significantly reduced in QDs compared with that in bulk materials due to the phonon-bottleneck effect.[45-48] Localized states on the QD surfaces and other defects also act as energy dissipation channels.[16,22,23] Therefore, it should be difficult to realize the step-like features of $\gamma(\hbar\omega)$. In fact, the experimentally observed $\gamma(\hbar\omega)$ shows an almost linear dependence, or an even more gradual increase for which it is difficult to clearly define the threshold.

The calculated results for the three features of $\gamma(\hbar\omega)$ are shown in **Fig. 5**. When $\gamma(\hbar\omega)$ increases gradually, the gain is significantly lowered. The gain for Slope 2 is only 3% (37% efficiency at ε_g = 0.95 eV). Note that even Slope 2 is considerably steeper than the experimental features.[16,20-27,29,30] The effect of the gradual increase is similar to that of a larger $\hbar\omega_{th}$ discussed in Sec. 2.2.1.

2. 2. 4 Influence of Solar Irradiation Intensity

The maximal power condition of a solar cell is determined from the trade-off relationship between V_{out} and J_{out}. A high V_{out} enhances the emission from the absorber represented by Eq. (3), and consequently decreases J_{out}. When a solar cell is used under concentrated irradiation, the influence of the emission is less significant relative to the absorption. Therefore, V_{out} at the maximal power condition (V_{max}) becomes higher, and thus the conversion efficiency is improved. The higher V_{max} at a given ε_g shifts the optimal ε_g to lower energy.

The lower optimal ε_g is advantageous for MEG cells, because more photons contribute to MEG. Therefore, the conversion efficiency of MEG cells increases more rapidly than that for no MEG with increasing solar irradiation intensity, i.e., the gain by MEG is more significant at higher intensity, as shown in **Fig. 6**. Even for Slope 2, a gain as high as 9% (50% efficiency at ε_g = 0.5 eV for Slope 2, and 41% at ε_g = 1.1 eV for no MEG) can be achieved at 1000 sun. However, even the efficiency for Step (59%) cannot reach the value of 3J-SCs (62%).[49] The values for Slope 1 and Slope 2

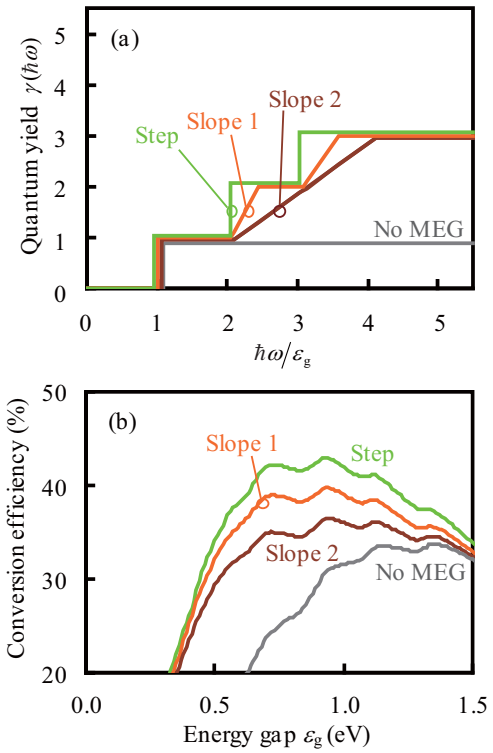

Fig. 5 (a) Model quantum yields ($\gamma(\hbar\omega)$) with different steepness. m_e/m_h = 0.04. (b) Conversion efficiency of MEG solar cells under 1 sun solar irradiation.

are further lowered to 55% and 50%, respectively.

The simple structure of MEG cells can potentially realize low areal cost comparable to that of conventional 1J-SCs. Therefore, one of the targets of MEG cells is utilization under non-concentrated solar irradiation for rooftop use. However, the conversion efficiency for Slope 2 at 1 sun is close to the value of 1J-SCs. Note again that even Slope 2 is considerably steeper than the experimental features. With respect to solar-concentrator systems, 3J-SCs using III-V compound semiconductors that provide significantly high conversion efficiency are mostly employed,[3-6,35,36] because the cell cost accounts for only 10-15% of the total system cost, so that the high cost of the 3J-SCs, due to their complicated multilayered structure, is not an issue.[50] Therefore, MEG cells are required to achieve conversion efficiency higher than that of 3J-SCs for solar-concentrator applications. However, even the ideal efficiency for Step is lower than the target value.

2. 3 Practical Upper Limit of Conversion Efficiency of MEG Solar Cells

We have clarified requisites to realize high conversion efficiency by utilizing MEG in QDs. InAs QDs embedded in $Al_xGa_{1-x}As_ySb_{1-y}$ is a possible candidate to fulfill the requisites for the QD materials, whereas PbSe or Si are not. However, the experimentally observed quantum yield of photon-to-carrier conversion, $\gamma(\hbar\omega)$, is far from that required to achieve high efficiency even for InAs QDs, due to energy dissipation processes competing against MEG.

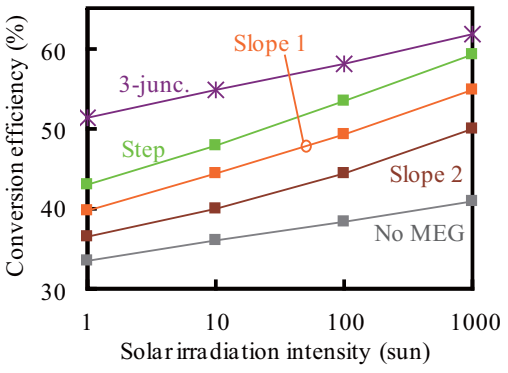

Fig. 6 Dependence of the conversion efficiency of MEG solar cells on the solar irradiation intensity. The model quantum yields ($\gamma(\hbar\omega)$) shown in Fig. 5(a) are used. The efficiency of a 3J-SC is also plotted for comparison.

In addition, the use of QDs involves various issues such as low light absorption, poor carrier transport, and significant interface recombination, which are not addressed in the present study. In consequence, it seems very difficult to realize conversion efficiency utilizing MEG in QDs higher than the value of conventional 1J-SCs, i.e., the S-Q limit under 1 sun solar irradiation, and those of 3J-SCs under concentrated solar irradiation.

3. Hot-carrier Solar Cells

In an HC-SC one photon generates one carrier, as is the case in conventional 1J-SCs. Instead, the photogenerated carriers are extracted before they are completely thermalized to utilize the carrier energy in excess of the bandgap of the absorber. For hot-carrier extraction, an HC-SC is equipped with energy-selective contacts (ESCs) on the both sides of the absorber, through which carriers at specific energy levels are extracted to metal electrodes, as illustrated in **Fig. 7**.[18,19]

In semiconductor QDs, when intervals of the quantum-confined energy levels are larger than the maximal phonon energy, a carrier at a high-energy level cannot relax to the next lower level with emission of one phonon. This effect is referred to as phonon bottleneck, and consequently thermalization can be significantly reduced compared with that in bulk materials.[45,46] In fact, thermalization times of several hundred picoseconds have been demonstrated in III-V compound semiconductor QDs.[47,48] Extraction of hot carriers through ESCs using double-barrier resonant-tunneling diodes (RTDs) consisting of Si QDs embedded in SiO_2 matrices[51] and GaAs/$Al_xGa_{1-x}As$

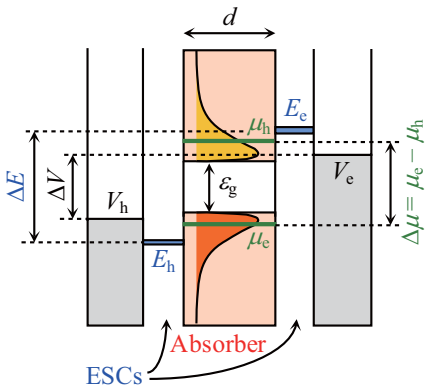

Fig. 7 Schematic configuration and energy diagram of an HC-SC.

quantum wells (QWs)[52] have been demonstrated.

There are three requisites that are unique to hot-carrier extraction to realize high conversion efficiency.[53] The first and most essential is a long thermalization time of photogenerated carriers in the absorber. A narrow energy-selection width of the ESC to reduce the entropy generation associated with hot-carrier extraction is the second requisite. The third one is a short equilibration time of carriers in the absorber due to elastic carrier-carrier interaction, so that empty states around the ESC levels from which carriers have been extracted are immediately filled by other carriers.

It has been found that under the ideal conditions, i.e., supposing no thermalization of carriers, an extremely narrow ESC width, and very rapid equilibration, the limiting conversion efficiency is as high as 65% under 1 sun solar irradiation and over 85% at 1000 sun (the reason for the significant dependence on the irradiation intensity is discussed later).[18,19] In the following, we conduct a qualitative analysis of the effect of a finite thermalization time using the established detailed-balance model.[54] Then, we construct a new rate-equation model to quantitatively evaluate the effect of all the three factors.[53]

3. 1 Effect of a Finite Thermalization Time of Photogenerated Carriers

3. 1. 1 Detailed Balance of Particle and Energy Fluxes

To derive the limiting conversion efficiency of an HC-SC, we consider the detailed balance of particle and energy fluxes, and entropy generation in the photovoltaic conversion process, as depicted in **Fig. 8**. In this subsection, the thermalization process is not explicitly involved in the model. In addition, the ideal conditions are assumed, i.e., an extremely narrow energy-selection width of the ESCs and very rapid equilibration of carriers, which simplifies derivation of the detailed-balance formulation described below. The effects of finite values for these parameters will be evaluated in Sec. 3.2. Complete light absorption at photon energies higher than the bandgap is postulated. Nonradiative recombination processes including Auger recombination, as well as impact ionization, are neglected.

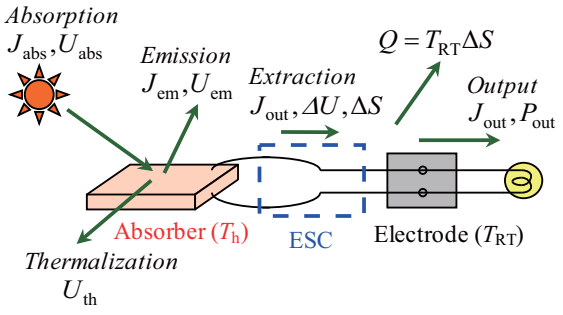

Fig. 8 Particle (J) and energy (U, Q, P_{out}) fluxes, and entropy generation (ΔS) involved in the present detailed-balance model for HC-SCs.

The output current density, J_{out}, is represented by the difference between the absorbed and emitted photon fluxes:

$$J_{out} = \int_{\varepsilon_g}^{\infty} d\varepsilon \left(j_{sun}(\varepsilon) - j_{em}(\varepsilon;\Delta\mu,T_c) \right) \equiv J_{abs} - J_{em}, \quad \cdots\cdots (10)$$

where $j_{sun}(\varepsilon)$ is again the solar spectral photon flux and ε_g the bandgap of the absorber. The assumption of very rapid carrier equilibration in the absorber ensures that the energy distribution of carriers in the absorber is characterized by quasi-Fermi levels in the CB and VB, μ_e and μ_h, respectively, similar to conventional solar cells, and a common carrier temperature, T_c, that is higher than T_{RT}. This in turn allows us to describe the emitted spectral photon flux, $j_{em}(\varepsilon;\Delta\mu,T_c)$, by the generalized Planck's law:[38,39]

$$j_{em}(\varepsilon;\Delta\mu,T_c) = \frac{2\pi}{h^3c^2} \frac{\varepsilon^2}{\exp\left[(\varepsilon-\Delta\mu)/(k_B T_c)\right]-1}, \quad \cdots\cdots (11)$$

$$\Delta\mu = \mu_e - \mu_h . \quad \cdots\cdots (12)$$

The balance of the energy fluxes describing absorption and emission, U_{abs} and U_{em}, respectively, determines the energy flux extracted from the absorber, ΔU:

$$\Delta U = U_{abs} - U_{em}, \quad \cdots\cdots (13)$$

$$U_{abs} = \int_{\varepsilon_{CV}}^{\infty} d\varepsilon\, \varepsilon\, j_{sun}(\varepsilon), \quad \cdots\cdots (14)$$

$$U_{em} = \int_{\varepsilon_{CV}}^{\infty} d\varepsilon\, \varepsilon\, j_{em}(\varepsilon;\Delta\mu,T_c). \quad \cdots\cdots (15)$$

The energy extracted from the absorber by one carrier equals the ratio of ΔU to J_{out}, which is exactly the difference between the ESC levels for electrons and holes, ΔE:

$$\Delta E = \Delta U / J_{out} . \quad \cdots\cdots\cdots\cdots\cdots\cdots (16)$$

When carriers in the absorber at T_c are extracted to the electrodes, in which the carrier temperature equals T_{RT}, entropy is generated, although the extremely narrow ESC width minimizes the amount of entropy generation, ΔS.[55] This is related to the other energy dissipation channel: thermodynamically derived unavoidable heat flux to the ambient surroundings, Q. Therefore, the output energy flux, P_{out}, is lower than ΔU by Q:[18]

$$\begin{aligned} Q &= T_{RT} \Delta S \\ &= J_{out} \left(\Delta E - J_{out} \Delta \mu \right) T_{RT} / T_c \\ &= \left(\Delta U - J_{out} \Delta \mu \right) T_{RT} / T_c , \end{aligned} \quad \cdots\cdots\cdots (17)$$

$$P_{out} = \Delta U - Q \equiv J_{out} V_{out} . \quad \cdots\cdots\cdots\cdots\cdots (18)$$

The conversion efficiency, η, is the ratio of P_{out} to the incident energy flux:

$$\eta = P_{out} \Big/ \int_0^\infty d\varepsilon \, \varepsilon \, j_{sun}(\varepsilon) . \quad \cdots\cdots\cdots\cdots\cdots (19)$$

We introduce the carrier retention time, τ_{re}, for comparison with the thermalization time, τ_{th}:

$$\tau_{re} = n_c \, d / J_{abs} , \quad \cdots\cdots\cdots\cdots\cdots\cdots (20)$$

where n_c and d are the carrier density in the absorber and the thickness of the absorber, respectively. A parabolic two-band model to represent the VB and CB in the absorber simplifies the relationship between n_c and μ_e:

$$n_c = 8\sqrt{2}\,\pi \, m_e^{3/2} / h^3 \int_{\varepsilon_g/2}^\infty d\varepsilon \, \sqrt{\varepsilon - \varepsilon_g/2} \frac{1}{\exp\left[(\varepsilon - \mu_e)/k_B T_c \right] + 1} . \quad \cdots\cdots\cdots\cdots\cdots (21)$$

Here, the origin of the energy axis is located at the center of the bandgap.

For the numerical evaluations in the following, $m_e = 0.04 m_0$ and $m_h = 0.4 m_0$ (m_0 denotes the electron rest mass), which are close to the values of $In_{0.53}Ga_{0.47}As$ and GaSb,[41] were used, because a small m_e, i.e., a small density of states (DOS) in the CB is required for high conversion efficiency.[54] Thin absorbers (d = 100 nm) were employed so that n_c was as large as possible.[54] The solar spectrum was approximated by a black-body emission at 5760 K.

3. 1. 2 Influence of the Carrier Retention Time

Figure 9(a) shows the dependence of the conversion efficiency on ε_g and T_c under 1000 sun solar irradiation. The optimal $\Delta\mu$ and corresponding n_c for each case are shown in Figs. 9(b) and (c), respectively. Over 70% conversion efficiency could be achieved at T_c = 1200-1800 K and ε_g smaller than 0.5 eV, with n_c in the order of 10^{18} cm^{-3}. However, in practice, the n_c value is limited to extract hot carriers, because τ_{re} must be much shorter than τ_{th}. If we consider τ_{th} = 1 ns, which is slightly longer than previously demonstrated values,[47,48] and τ_{re} = 100 ps, then n_c is calculated from Eq. (20) to be in the order of 10^{15} cm^{-3}, which is extremely smaller than that under the conditions for high efficiency.

To evaluate the influence of n_c on the conversion efficiency, we calculated the conversion efficiency as a function of n_c. **Figure 10**(a) shows that the conversion efficiency has an approximately linear dependence on log[n_c] up to $n_c = 10^{17}$ cm^{-3}. After showing a maximum, the efficiency rapidly decreases in the larger n_c range. When T_c is higher, a higher value of maximal efficiency appears at a larger n_c: 56% (T_c = 600 K, $n_c = 4 \times 10^{17}$ cm^{-3}), 71% (T_c = 1200 K, $n_c = 7 \times 10^{17}$ cm^{-3}), and 75% (T_c = 1800 K, $n_c = 9 \times 10^{17}$ cm^{-3}). However, the practically achievable conversion efficiency is considerably lower than these values, because n_c is limited to the order of 10^{15} cm^{-3}. The values for $n_c = 5 \times 10^{15}$ cm^{-3} corresponding to d = 100 nm, 1000 sun solar irradiation intensity and τ_{re} = 93 ps are 43, 56, and 59% at T_c = 600, 1200, and 1800 K, respectively.

Although thermalization is excluded in this subsection, there are still two channels of energy dissipation that restrict the conversion efficiency; emission from the absorber represented by U_{em}, and the unavoidable heat flux to the ambient surroundings, Q. The former affects both J_{out} and V_{out}, and the effect is evaluated by U_{em}/U_{abs}. The measure of the latter can

be simplified as:

$$Q/(U_{abs}-U_{em})=(1-\Delta\mu/\Delta E)\,T_{RT}/T_c \quad \cdots\cdots (22)$$

This is a straightforward expression indicating that the energy dissipation by Q affects only V_{out}. The dependence of these measures on n_c is shown in Fig. 10(b).

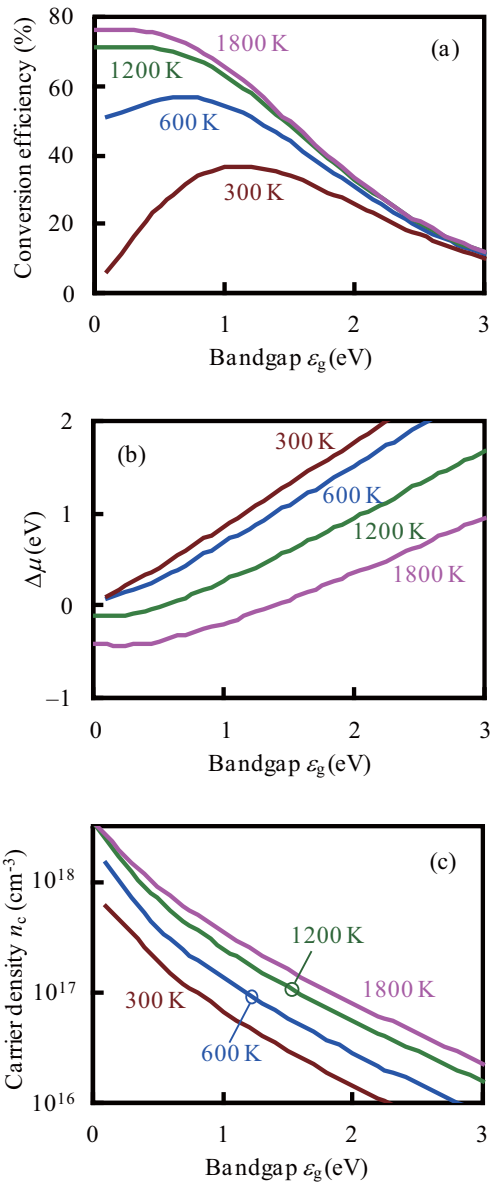

Fig. 9 Dependence of the (a) conversion efficiency (b) $\Delta\mu \equiv \mu_e - \mu_h$, and (c) carrier density (n_c) (optimized for each case) of HC-SCs on the bandgap of the absorber ε_g, and the carrier temperature (T_c = 300, 600, 1200, 1800 K). $m_e = 0.04m_0$, $m_h = 0.4m_0$, no thermalization of carriers, 1000 sun.

With increasing n_c, $\Delta\mu$ becomes larger. The linear dependence of $\Delta\mu$ on log[n_c] at a given T_c is derived from Eq. (21) using the Boltzmann approximation. Therefore, it is found from Eq. (22) that $Q/(U_{abs} - U_{em})$ is linearly reduced depending on log[n_c], as shown in Fig. 10(b). It is also found that $Q/(U_{abs} - U_{em})$ is a decreasing function of T_c at a given n_c, because the change in $\Delta\mu$ with T_c has only a slight effect relative to the factor of $1/T_c$.

The value of U_{em}/U_{abs} is close to zero up to n_c = 10^{16} cm^{-3} and rapidly increases in the larger n_c range. At a given n_c, U_{em}/U_{abs} is lower for a higher T_c, which is the reason why the maximal efficiency appears at a larger n_c for a higher T_c, and does not contradict the fact that emission from a heated material is more intense at a higher temperature. In a heated material, more carriers are generated thermally at a higher temperature, whereas the influence of T_c with a given n_c is evaluated here.

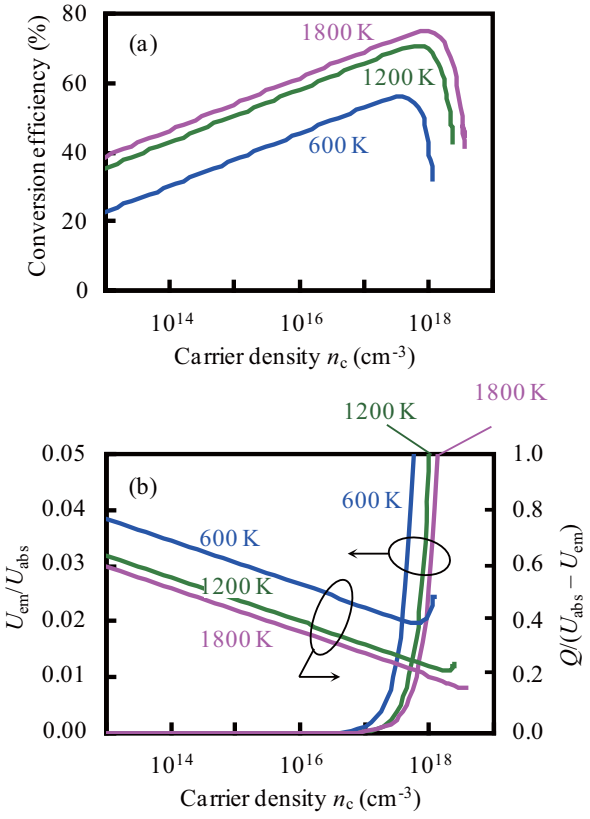

Fig. 10 (a) Conversion efficiency of HC-SCs as a function of the carrier density (n_c), and the carrier temperature (T_c = 600, 1200, 1800 K). (b) Influence of the emission (U_{em}) and unavoidable heat flux (Q) as a function of the carrier density (n_c). ε_g = 0.5 eV, $m_e = 0.04m_0$, $m_h = 0.4m_0$, no thermalization of carriers, 1000 sun.

However, the effect of U_{em}/U_{abs} is negligible in the practically achievable n_c range up to 10^{15} cm^{-3}, even at T_c = 600 K. Therefore, the conversion efficiency is dominated by Q and linearly dependent on n_c in this n_c range, as shown in Fig. 10(a). At a larger n_c, U_{em}/U_{abs} has a significant effect on the efficiency, leading to the rapid decrease in the efficiency.

In Eq. (21), the use of a bulk material is assumed, whereas QDs and other low-dimensional materials are attractive candidates for use as the absorbers as first mentioned in this section. Even using the DOS of 0-, 1- or 2-dimensional structures, linear dependence of $\Delta\mu$ on $\log[n_c]$ is also derived from the relationship between μ_e, μ_h, and n_c, similar to Eq. (21). Therefore, the conversion efficiency is still linearly dependent on $\log[n_c]$.

The influence of the solar irradiation intensity with practically achievable τ_{re} values is similarly interpreted. **Figure 11**(a) shows a comparison of the results at a constant T_c of 1200 K for different intensities: non-, 1000 times- and the maximal (approx. 46000 times-) concentration. In the shorter τ_{re} range up to 1 ns, the conversion efficiency is linearly dependent on $\log[\tau_{re}]$, and the conversion efficiency at a given τ_{re} is higher for a higher intensity. With increasing τ_{re}, the efficiency reaches the maximal value, followed by a rapid decrease. The maximum appears at a shorter τ_{re}, but the value is higher when the intensity is higher.

The influence of the solar irradiation intensity can be more apparently interpreted by calculating the efficiency as a function of n_c for different intensities. The results with the effect on Q and U_{em} are shown in Figs. 11(b) and 11(c), respectively. As long as U_{em} is negligible, there appears to be no significant difference in Q, and consequently in the efficiency at different irradiation intensities, because Q is dominated by $\Delta\mu$ as shown in Eq. (22), and hence by n_c. Therefore, the reason why the efficiency is higher under more intense irradiation when τ_{re} is an achievable value shorter than 1 ns, as shown in Fig. 11(a), is simply a larger n_c that is proportional to the product of τ_{re} and the irradiation intensity.

However, the conversion efficiency starts to decrease at a smaller n_c for a lower irradiation intensity, because the relative impact of U_{em} is inversely proportional to the solar irradiation intensity. This is the reason why the maximal value of the efficiency is higher for a higher irradiation intensity, with the supposition of no limitation of τ_{re} and n_c arising from thermalization, i.e., no thermalization, and is different from the reason for the intensity-dependence of the efficiency at a practically achievable τ_{re} value mentioned above. The influence of the irradiation intensity on the maximal value of the efficiency has been more explicitly elucidated in terms of entropy generation caused by the mismatch between the absorption and emission

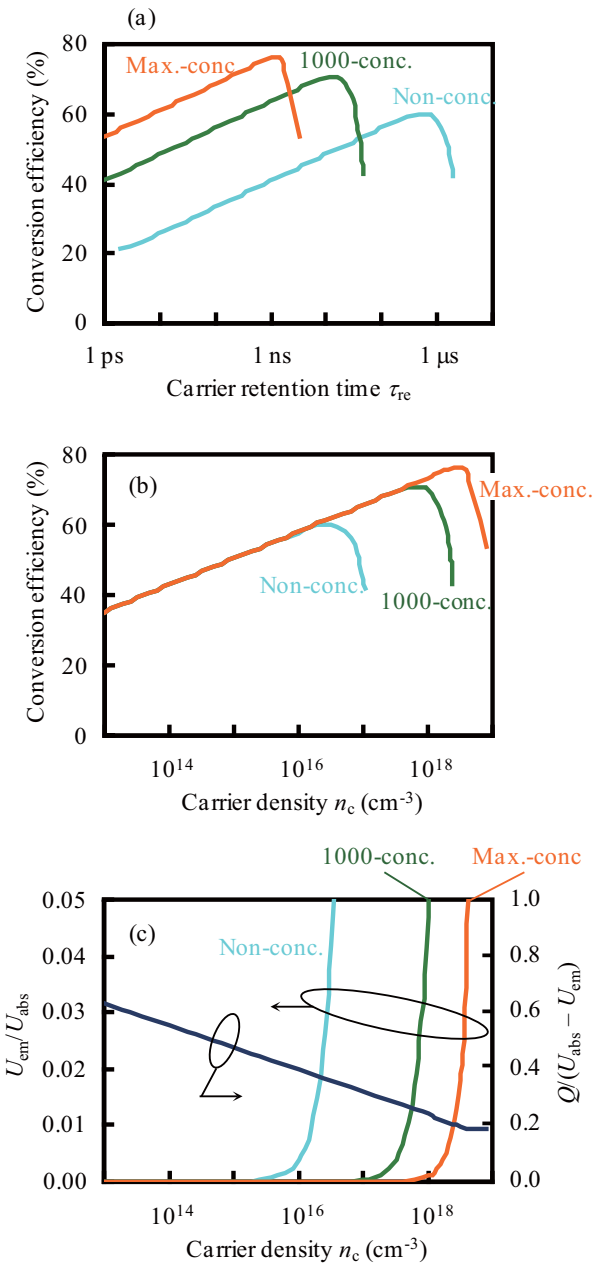

Fig. 11 Conversion efficiency of HC-SCs as a function of the carrier retention time (τ_{re}) and solar irradiation intensity (non-, 1000 times- and the maximal concentration). ε_g = 0.5 eV, m_e = 0.04m_0, m_h = 0.4m_0, d = 100 nm, no thermalization of carriers, T_c = 1200 K.

étendues, which is analogous to the adiabatic expansion of ideal gas.[56,57]

3. 2 Quantitative Evaluation of the Practical Factors

3. 2. 1 A Rate-equation Model

We formulate a rate equation to describe the energy distribution of electrons in the CB, $n_e(\varepsilon)$, and quantitatively involve the effects of the finite thermalization time, τ_{th}, and equilibration time, τ_{eq}, in the absorber, and the energy selection widths of the ESCs, w_{esc}. For simplification, holes in the VB are assumed to be immediately thermalized and obey the Fermi-Dirac statistics at T_{RT}, because most of the absorbed photon energy is stored in the electron subsystem and consequently thermalization of holes has a slight effect on the conversion efficiency when m_h is much larger than m_e.[54]

In the steady-state operation of an HC-SC, electrons in the CB are constantly generated by photoabsorption. Some of these electrons radiatively recombine with holes and the remaining are extracted to the electrode. In addition, $n_e(\varepsilon)$ is affected by equilibration and thermalization. Considering these processes, the time evolution of $n_e(\varepsilon)$ is represented as:

$$\frac{dn_e(\varepsilon)}{dt} = -\frac{n_e(\varepsilon) - f(\varepsilon;\mu_{eq},T_{eq})\rho_e(\varepsilon)}{\tau_{eq}} - \frac{n_e(\varepsilon) - f(\varepsilon;\mu_{th},T_{RT})\rho_e(\varepsilon)}{\tau_{th}} + G_e(\varepsilon) - R_e(\varepsilon) - E_e(\varepsilon;V_e), \quad \cdots\cdots\cdots\cdots (23)$$

where $G_e(\varepsilon)$, $R_e(\varepsilon)$, and $E_e(\varepsilon,V_e)$ are the generation, radiative recombination, and extraction rates, respectively, $f(\varepsilon;\mu,T)$ the Fermi-Dirac distribution function with a quasi-Fermi level μ and a temperature T, and $\rho_e(\varepsilon)$ the DOS per unit area in the CB (not per unit volume). Impact ionization and Auger recombination have been confirmed to be negligible under the conditions employed, although the former is generally significant at a high T_c and the latter at a large n_c.[58] The Fermi level in the negative electrode, V_e, directly affects $E(\varepsilon,V_e)$ (see Eq. (29)).

Here, τ_{th} is dealt with as a given constant, because in reality it is only slightly dependent on n_c and T_c, as long as T_c is sufficiently higher than the Debye temperature and n_c is not sufficiently large to cause saturation effects.[59-61] The dependence of τ_{eq} on n_c and T_{eq} is also neglected for a straightforward interpretation, although these parameters intricately affect τ_{eq}.[62] The feasibility of the τ_{eq} and τ_{th} values used for numerical evaluation will be examined later in relation to the resultant operating states.

The first term in the right-hand side of Eq. (23) describes the equilibration process, in which the nonequilibrium $n_e(\varepsilon)$ evolves toward the equilibrated distribution characterized by the Fermi-Dirac statistics at T_{eq}, which is higher than T_{RT}. This process is due to electron-electron elastic scattering (equilibration within the electron subsystem; electron-phonon scattering is excluded). Therefore, the total density and energy of the electrons are conserved:

$$\int_0^\infty d\varepsilon\, f(\varepsilon;\mu_{eq},T_{eq})\rho_e(\varepsilon) = \int_0^\infty d\varepsilon\, n_e(\varepsilon), \quad \cdots\cdots (24)$$

$$\int_0^\infty d\varepsilon\, \varepsilon\, f(\varepsilon;\mu_{eq},T_{eq})\rho_e(\varepsilon) = \int_0^\infty d\varepsilon\, \varepsilon\, n_e(\varepsilon). \quad \cdots\cdots\cdots\cdots (25)$$

The origin of the energy axis is located at the bottom of the CB for simple expressions. These relationships determine the values of μ_{eq} and T_{eq}.

In contrast, the thermalization process described by the second term originates from inelastic scattering of electrons with phonons at T_{RT} (i.e., equilibration between electrons and phonons). Therefore, $n_e(\varepsilon)$ evolves toward the distribution at T_{RT} and the total electron energy dissipates in this process, although conservation of the total electron density holds:

$$\int_0^\infty d\varepsilon\, f(\varepsilon;\mu_{th},T_{RT})\rho_e(\varepsilon) = \int_0^\infty d\varepsilon\, n_e(\varepsilon). \quad \cdots\cdots (26)$$

A parabolic two-band model is again used to describe $\rho_e(\varepsilon)$, $G_e(\varepsilon)$, and $R_e(\varepsilon)$. An electron with an energy ε is generated by absorbing a photon with an energy $\hbar\omega = (\varepsilon_g + (1 + m_e/m_h)\,\varepsilon$. Therefore, $G_e(\varepsilon)$ is expressed as:

$$G(\varepsilon) = j_{sun}(\varepsilon_g + (1 + m_e/m_h)\,\varepsilon). \quad \cdots\cdots\cdots (27)$$

The generalized Planck's law[38,39] can be modified to determine $R_e(\varepsilon)$ using the occupation probability in the CB, $n_e(\varepsilon)/\rho_e(\varepsilon)$, instead of the Fermi-Dirac distribution function:

$$R_e(\varepsilon)=\frac{2\pi}{h^3c^2}\frac{\left(\varepsilon_g+(1+m_e/m_h)\varepsilon\right)^2}{(\rho_e(\varepsilon)/n_e(\varepsilon)-1)\exp\left[\left(\varepsilon_g+m_e/m_h\,\varepsilon+\mu_h\right)/\left(k_B T_{RT}\right)\right]-1}. \quad \cdots\cdots\cdots\cdots (28)$$

When an RTD consisting of semiconductor QDs surrounded by a barrier material is used as the ESC, electrons of a specific energy in the absorber can be extracted via the quantum-confined states in the QDs. However, in practice, size non-uniformity of the QDs causes a finite value of w_{esc}. Assuming that the distribution of the quantum-confined levels is represented by a Gauss function centered at E_{esc}, then $E_e(\varepsilon;V_e)$ is derived using the standard expression of a tunneling current:[63]

$$E_e(\varepsilon;V_e)=A\frac{2}{\pi\, w_{esc}}\exp\left[-\left(\frac{\varepsilon-E_{esc}}{w_{esc}/2}\right)^2\right] \varepsilon\left(n_e(\varepsilon)/\rho_e(\varepsilon)-f(\varepsilon;V_e,T_{RT})\right), \quad \cdots\cdots\cdots\cdots (29)$$

where $f(\varepsilon;V_e,T_{RT})$ is the Fermi-Dirac distribution function in the negative electrode. The proportionality constant A is dependent on the detailed structure of the ESC, such as the areal density of the QDs, and the thickness and potential height of the barriers.[64]

The total extraction rate equals the difference between the total generation and recombination rates:

$$\int_0^\infty d\varepsilon\; E_e(\varepsilon;V_e)=\int_0^\infty d\varepsilon\; G_e(\varepsilon)-\int_0^\infty d\varepsilon\; R_e(\varepsilon). \quad \cdots\cdots\cdots\cdots (30)$$

Therefore, it is an additional requisite for high conversion efficiency to realize an A value that satisfies Eq. (30). The expression of the total energy-extraction rate is affected by the energy dissipation caused by thermalization:

$$\int_0^\infty d\varepsilon\;\varepsilon\; E_e(\varepsilon;V_e)=\int_0^\infty d\varepsilon\;\varepsilon\; G_e(\varepsilon)-\int_0^\infty d\varepsilon\;\varepsilon\; R_e(\varepsilon) -\int_0^\infty d\varepsilon\;\varepsilon\;\frac{n_e(\varepsilon)-f(\varepsilon;\mu_{th},T_{RT})\rho_e(\varepsilon)}{\tau_{th}}. \quad \cdots\cdots\cdots\cdots (31)$$

By solving the simultaneous equations of $dn_e(\varepsilon)/dt = 0$ and Eqs. (30) and (31), $n_e(\varepsilon)$ and other values in a steady-state operation are then determined. The Fermi level in the positive electrode, V_h, equals μ_h, because the hole temperature is assumed to be T_{RT}. Thus, the conversion efficiency, η, is the product of the output voltage and the total extraction rate divided by the total incident power:

$$\eta=\left(V_e-V_h\right)\int_0^\infty d\varepsilon\; E_e(\varepsilon;V_e)\Big/\int_0^\infty d\varepsilon'\,\varepsilon'\, j_{sun}(\varepsilon'). \quad \cdots\cdots\cdots\cdots (32)$$

In the following numerical procedures, $m_e = 0.04m_0$ and $m_h = 0.4m_0$ were again used. The absorber thickness was set at 500 nm, which is more practical than the value used in the previous subsection. The AM1.5G solar spectrum was used up to 10 sun solar irradiation intensity, and AM1.5D for higher intensity.[40]

3. 2. 2 Detrimental Impact of the Practical Factors

Figure 12(a) shows the dependence of the conversion efficiency on w_{esc}. When w_{esc} approaches zero, the entropy generation associated with hot carrier extraction is minimized.[55] With increasing w_{esc}, the entropy generation increases and the conversion efficiency is consequently lowered. Another interpretation is that the influence of the reverse flow of electrons represented by a negative value of $n_e(\varepsilon)/\rho_e(\varepsilon) - f(\varepsilon;V_e,T_{RT})$ in Eq. (29) at a lower ε is more significant when w_{esc} is larger.[65] If the target of the conversion efficiency is relatively 5% lower than the value at $w_{esc} = 0$, a w_{esc} around 0.1 eV is required.

A sufficiently narrow peak in a current-voltage relationship has been demonstrated using an RTD consisting of InAs QDs with an electrode of several square micrometers.[66] However, it still remains a challenge to realize a small w_{esc} using practically larger sized devices. Moreover, it has not yet been clarified whether an appropriate value of the proportionality constant A in Eq. (29) can be realized.[64]

As long as there is a sufficient supply of electrons to the empty states located around the ESC level, τ_{eq} does not have a significant effect on the efficiency, as shown in Fig. 12(b). However, at a longer τ_{eq}, $n_e(\varepsilon)$ is much lower at the ESC level, which limits $E_e(\varepsilon;V_e)$ and consequently lowers the conversion efficiency. The target value of τ_{eq} to prevent such a rate-limitation is in the order of 1/1000 of τ_{th} (e.g., several picoseconds at τ_{th} = 1 ns).

The value of n_c for τ_{th} = 1 ns and 1000 sun has been confirmed again to be in the order of 10^{15} cm^{-3}, using the results of the present rate-equation model. In bulk GaAs, τ_{eq} at a n_c of approximately 10^{15} cm^{-3} has been found to be several picoseconds,[62] which is close to the target value of τ_{th}/1000. However, when τ_{th} is shorter and/or the irradiation intensity is lower a sufficiently short τ_{eq} would be difficult to realize, because n_c is proportional to the product of τ_{th} and the solar irradiation intensity,[54] whereas τ_{eq} is longer at a lower n_c.[62]

The most dominant factor is τ_{th}, as shown in Fig. 12(c). To exceed the S-Q limit under 1 sun solar irradiation (34%), a τ_{th} longer than 1 ns is required. Under 1000 sun solar irradiation, conversion efficiency higher than the S-Q limit (41%) can be achieved at a τ_{th} of several tens of picoseconds. However, the target must be the conversion efficiency of 3J-SCs (62%),[49] as discussed in Sec. 2.2.4. To achieve such a high efficiency, a τ_{th} longer than 10 ns is required. More detailed analysis has revealed that the unavoidable heat flux to the ambient surroundings, which is related to the entropy generation associated with hot-carrier extraction, is the major energy dissipation channel, as quantitatively evaluated in Sec. 3.1, whereas the energy dissipation caused by the thermalization represented by the second term in the right-hand side of Eq. (23) is sufficiently reduced under the present conditions.[67]

The use of QD arrays in the absorber is a potential solution to realize a long τ_{th}, as mentioned above. However, the experimentally demonstrated τ_{th} values of several hundreds of picoseconds at low ambient temperatures are not sufficiently long.[47,48] Furthermore, immediate equilibration is a more difficult requisite than that in bulk materials, because the average electron number per QD is much less than unity when n_c equals 10^{15} cm^{-3}. Miniband formation originating from electronic coupling between neighboring QDs leads to an acceleration of the equilibration, in addition to improvements of light absorption and carrier transport properties in the absorber that are not addressed in the present model. However, this also leads to a shorter τ_{th}. Therefore, it is a more serious issue whether all the functions of the absorber are compatible with each other.

The dependence on τ_{th} is due to the approximately linear dependence of conversion efficiency on log[n_c], in which n_c is proportional to the product of τ_{th} and the solar irradiation intensity,[54] as long as the energy

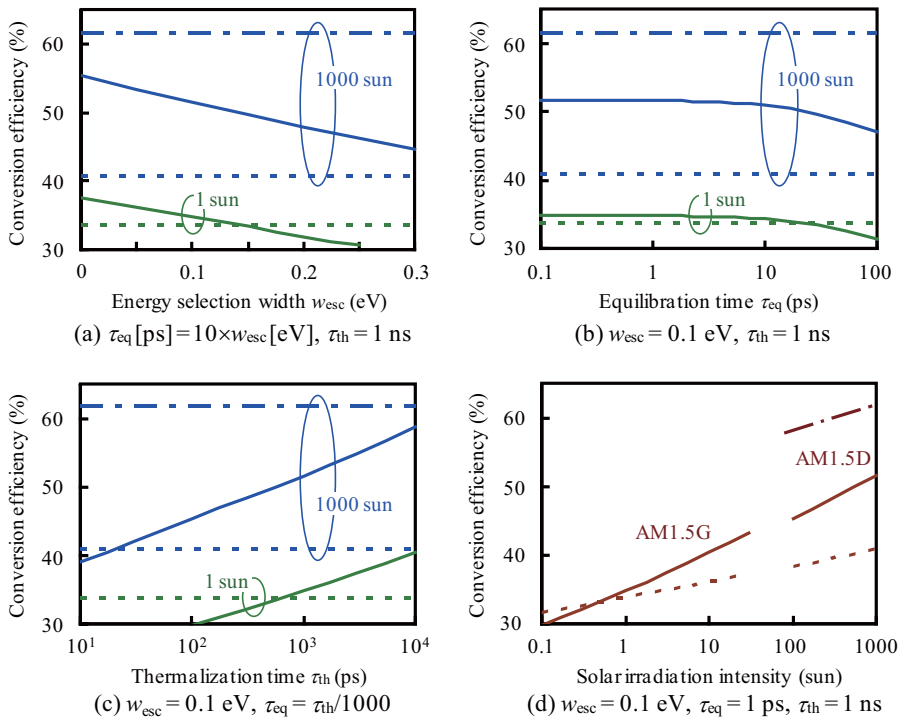

Fig. 12 Dependence of the conversion efficiency on (a) the ESC energy selection width (w_{esc}), (b) the equilibration time (τ_{eq}) and (c) thermalization time (τ_{th}) in the absorber, and (d) the solar irradiation intensity. Broken lines and dashed-dotted lines indicate the limiting efficiencies of 1J-SCs (S-Q limit) and 3J-SCs, respectively.

dissipation caused by emission is not significant, as discussed in Sec. 3.1.2. Therefore, the dependence on the intensity shown in Fig. 12(d) is very close to the τ_{th} dependence in Fig. 12(c). For example, the efficiency at τ_{th} = 100 ps and 1000 sun is almost the same as that at τ_{th} = 1 ns and 100 sun.

The thickness of the absorber similarly affects the conversion efficiency. When the absorption coefficient is low, and hence twice the thickness is required for sufficient light absorption, n_c is halved at a given τ_{th} and solar irradiation intensity, which results in lowering of the efficiency. This is equivalent to halving τ_{th} or the intensity at a given thickness.

3. 3 Practical Upper Limit of Conversion Efficiency of HC-SCs

We have evaluated the effects of the three practical factors unique to HC-SCs. The energy dissipation caused by thermalization of photogenerated carriers could be sufficiently reduced if a thermalization time (τ_{th}) of 1 ns could be realized. Instead, another energy dissipation channel, thermodynamically unavoidable heat flux to the ambient surroundings, which is related to the entropy generation associated with hot-carrier extraction, has a serious impact on the conversion efficiency.[67] Thus, the conversion efficiency is close to that of 1J-SCs, i.e. the S-Q limit under 1 sun solar irradiation, and lower than that of 3J-SCs under 1000 sun solar irradiation. In addition, the target values of 0.1 eV for the ESC energy selection width (w_{esc}) and a carrier equilibration time (τ_{eq}) in the order of τ_{th}/1000 seem difficult to realize. Analysis on specific materials and using other models for the thermalization process have drawn similar conclusions.[68-71]

Theoretical investigations to address the issues on HC-SCs are in progress. Modification of phonon dispersion to suppress energy dissipation from optical phonons to acoustic phonons could extend the thermalization time of hot carriers.[72,73] Two approaches to solve the issues in the ESCs have been proposed. One is the use of an absorber consisting of QWs that has a function of energy-selective carrier transport.[74] The other is extraction of high-energy photons instead of hot carriers, i.e., the use of hot luminescence from an absorber coupled with an optical resonator to convert the solar spectrum to a monochromatic light that is incident to a conventional 1J-SC.[75] Extraction of hot carriers from an absorber that has an intermediate-band (IB) can relax the requisite of thermalization time, because a smaller output current density reduces the entropy generation associated with hot-carrier extraction compared with those for single-gap absorbers.[67,76,77] However, specific implementations have not yet been carried out, so that the feasibility of these new ideas has yet to be clarified.

4. Concluding Remarks

Multiple exciton generation (MEG) solar cells and hot-carrier solar cells (HC-SCs) have been expected to provide very high conversion efficiency. The concepts of these types have previously been proposed, and detailed-balance calculations to find the limiting conversion efficiency under the ideal conditions have been performed. However, the detrimental effects of various practical factors, i.e., energy dissipation processes that could be eliminated in principle but are practically unavoidable, have not been clarified.

We have constructed new detailed-balance models to evaluate the effects of some of the practical factors and explore the feasibility of MEG solar cells and HC-SCs with respect to currently used solar cells. The simple structures of these two types can potentially realize low areal costs comparable to those of conventional single-junction solar cells (1J-SCs). Therefore, one of the targets of these cells is rooftop use under non-concentrated solar irradiation. Another target is for solar-concentrator systems, for which triple-junction solar cells (3J-SCs) are the competitors.

The results of the present evaluation are not encouraging. The limiting conversion efficiency is significantly lowered under practical conditions compared with those for the ideal cases to be close to that for 1J-SCs, i.e., the Shockley-Queisser (S-Q) limit under non-concentrated solar irradiation, and lower than that of 3J-SCs under 100-1000 times-concentrated solar irradiation. In addition, other factors not involved in the present models remain, which most likely have detrimental impacts on the conversion efficiency. In particular, the carrier transport properties of the absorbers generally have a significant effect on the conversion efficiency.

To design suitable carrier-carrier and carrier-phonon interactions that govern the phenomena of MEG and hot-carrier thermalization is a challenging yet fascinating problem in condensed matter physics. However, from the viewpoint of practical application, we must recognize that it appears very difficult for MEG solar cells and HC-SCs to compete against

existing single-junction solar cells that operate based on the conventional mechanism, such as Si and $CuIn_{1-x}Ga_xSe$ (CIGS) cells for rooftop use, and 3J-SCs using III-V compound semiconductors coupled with solar concentrators.

References

(1) Green, M. A., *Third Generation Photovoltaics* (2003), pp.35-58., Springer-Verlag
(2) Shockley, W. and Queisser, H. J., *J. Appl. Phys.*, Vol.32 (1961), pp.510-519.
(3) Green, M. A., Emery, K., Hishikawa, Y., Warta, W. and Dunlop, E. D., *Prog. Photovol.: Res. Appl.*, Vol.19 (2011), pp.565-572.
(4) Yoshida, A., Agui, T., Nakaido, K., Murasawa, K., Juso, H., Sasaki, K. and Takamoto, T., *Tech. Dig. 21st Photovoltaic Science and Engineering Conference* (2011), 4B-4O-01.
(5) Yamaguchi, M., Suzuki, H., Oshita, Y., Kojima, N. and Takamoto, T., *Proc. 35th IEEE Photovoltaic Specialists Conference* (2010), pp.1237-1242.
(6) King, R. R., Dhusari, D., Boca, A., Larrabee, D., Liu, X.-Q., Hong, W., Fetzer, C. M., Law, D. C. and Karam, N. H., *Prog. Photovolt.: Res. Appl.*, Vol.19 (2011), pp.797-812.
(7) Luque, A. and Martí, A., *Phys. Rev. Lett.*, Vol.78 (1997), pp.5014-5017.
(8) Luque, A. and Martí, A., *Adv. Mater.*, Vol.22 (2010), pp.160-174.
(9) Trupke, T. and Green, M. A., *J. Appl. Phy.*, Vol.92 (2002), pp.4117-4122.
(10) Wang, W., Lin, A. S. and Phillips, J. D., *Appl. Phys. Lett.*, Vol.95 (2009), 011103.
(11) López, N., Reichertz, L. A., Yu, K. M., Campman, K. and Walukiewicz, W., *Phys. Rev. Lett.*, Vol.106 (2011), 028701.
(12) Martí, A., Antolín, E., Stanley, C. R., Farmer, C. D., López, N., Díaz, P., Cánovas, E., Linares, P. G. and Luque, A., *Phys. Rev. Lett.*, Vol.97 (2006), 247701.
(13) Okada, Y., Morioka, T., Yoshida, K., Oshima, R., Shoji, Y., Inoue, T. and Kita, T., *J. Appl. Phys.*, Vol.109 (2011), 024301.
(14) Kim, S. J., Kim, W. J., Cartwright, A. N. and Prasad, P. N., *Appl. Phy. Lett.*, Vol.92 (2008), 191107.
(15) Sukhovatkin, V., Hinds, S., Brzozowski, L. and Sargent, E. H., *Science*, Vol.324 (2009), pp.1542-1544.
(16) Beard, M. C., *J. Phys. Chem. Lett.*, Vol.2 (2011), pp.1282-1288.
(17) Trupke, T., Green, M. A. and Würfel, P., *J. Appl. Phys.*, Vol.92 (2002), pp.1668-1674.
(18) Ross, R. T. and Nozik, A. J., *J. Appl. Phys.*, Vol.53 (1982), pp.3813-3818.
(19) Würfel, P., *Solar Energy Mater. Solar Cells*, Vol.46 (1997), pp.43-52.
(20) Hardman, S. J. O., Graham, C. M., Stubbs, S. K., Spencer, B. F., Seddon, E. A., Fung, H.-T., Gardonio, S., Sirotti, F., Silly, M. G., Akhtar, J., O'Brien, P., Binks, D. J. and Flavella, W. R., *Phys. Chem. Chem. Phys.*, Vol.13 (2011), pp.20275-20283.
(21) Stewart, J. T., Padilha, L. A., Qazilbash, M. M., Pietryga, J. M., Midgett, A. G., Luther, J. M., Beard, M. C., Nozik, A. J. and Klimov, V. I., *Nano Lett.*, Vol.12 (2012), pp.622-628.
(22) McGuire, J. A., Sykora, M., Joo, J., Pietryga, J. M. and Klimov, V. I., *Nano Lett.*, Vol.10 (2010), pp.2049-2057.
(23) Midgett, A. G., Hillhouse, H. W., Hughes, B. K., Nozik, A. J. and Beard, M. C., *J. Phys. Chem. C*, Vol.114 (2010), pp.17486-17500.
(24) Murphy, J. E., Beard, M. C., Norman, A. G., Ahrenkiel, S. P., Johnson, J. C., Yu, P., Mićić, O. I., Ellingson, R. J. and Nozik, A. J., *J. Am. Chem. Soc.*, Vol.128 (2006), pp.3241-3247.
(25) Schaller, R. D., Petruska, M. A. and Klimov, V. I., *Appl. Phys. Lett.*, Vol.87 (2005), 253102.
(26) Kobayashi, Y., Udagawa, T. and Tamai, N., *Chem. Lett.*, Vol.38 (2009), pp.830-831.
(27) Schaller, R. D., Pietryga, J. M. and Klimov, V. I., *Nano Lett.*, Vol.7 (2007), pp.3469-3476.
(28) Pijpers, J. J. H., Hendry, E., Milder, M. T. W, Fanciulli, R., Savolainen, J., Herek, J. L., Vanmaekelbergh, D., Ruhman, S., Mocatta, D., Oron, D., Aharoni, A., Banin, U. and Bonn, M., *J. Phys. Chem. C*, Vol.111 (2007), pp.4146-4152.
(29) Stubbs, S. K., Hardman, S. J. O., Graham, D. M., Spencer, B. F., Flavell, W. R., Glarvey, P., Masala, O., Pickett, N. L. and Binks, D. J., *Phys. Rev. B*, Vol.81 (2010), 081303.
(30) Beard, M. C., Knutsen, K. P., Yu, P., Luther, J. M., Song, Q., Metzger, W. K., Ellingson, R. J. and Nozik, A. J., *Nano Lett.*, Vol.7 (2007), pp.2506-2512.
(31) Pijpers, J. J. H., Ulbricht, R., Tielrooij, K. J., Osherov, A., Golan, Y., Delerue, C., Allan, G. and Bonn, M., *Nature Phys.*, Vol.5 (2009), pp.811-814.
(32) Nozik, A. J., *Physica E*, Vol.14 (2002), pp.115-120.
(33) Takeda, Y. and Motohiro, T., *Solar Energy Mater. Solar Cells*, Vol.94 (2010), pp.1399-1405.
(34) Takeda, Y. and Motohiro, T., *Proc. 25th European Photovoltaic Solar Energy Conference* (2010), pp.207-211.
(35) Araki, K., Kondo, M., Uozumi, H., Ekins-Daukes, N. J., Egami, T., Hiramatsu, M., Miyazaki, Y. and Yamaguchi, M., *Solar Energy Mater. Solar Cells*, Vol.90 (2006), pp.3320-3326.
(36) Luque, A., *J. Appl. Phys.,* Vol.110 (2011), 031301.
(37) Hanna, M. C. and Nozik, A. J., *J. Appl. Phys.*, Vol.100 (2006), 074510.
(38) Würfel, P., *J. Phys. C: Solid State Phys.*, Vol.15 (1982), pp.3967-3985.
(39) Spirkl, W. and Ries, H., *Phys. Rev. B*, Vol.52 (1995), pp.11319-11325.
(40) "Solar Spectral Irradiance: Air Mass 1.5", <http://rredc.nrel.gov/solar/spectra/am1.5/>, (accessed 2012-7-17).

(41) Madelung, O., *Semiconductors: Data Handbook* (2003), Springer-Verlag.
(42) Velizhanin, K. A. and Piryatinski, A., *Phys. Rev. Lett.*, Vol.106 (2012), 207401.
(43) Schulze, F., Schoth, M., Woggon, U., Knorr, A. and Weber, A., *Phys. Rev. B*, Vol.84 (2011), 125318.
(44) Nishikawa, K., Takeda, Y., Yamanaka, K., Motohiro, T., Sato, D., Ota, J., Miyashita, N. and Okada, Y., *J. Appl. Phys.*, Vol.111 (2012), 044325.
(45) Bockelmann, B. and Bastard, G., *Phys. Rev. B*, Vol.42 (1990), pp.8947-8951.
(46) Benisty, H., Sotomayor-Torres, C. M. and Weisbuch, C., *Phys. Rev. B*, Vol.44 (1991), pp.10945-10948.
(47) Urayama, J., Norris, T. B., Singh, J. and Bhattacharya, P., *Phys. Rev. Lett.*, Vol.86 (2001), pp.4930-4933.
(48) Heitz, R., Born, H., Guffarth, G., Stier, O., Schliwa, A., Hoffmann, A. and Bimberg, D., *Phys. Rev. B*, Vol.64 (2001), 241305.
(49) Guter, W., Schöne, J., Philipps, S. P., Steiner, M., Siefer, G., Wekkeli, A., Welser, E., Oliva, E., Bett, A. W. and Dimroth, F., *Appl. Phys. Lett*., Vol.94 (2009), 223504.
(50) Araki, K., *private commun.* (2007).
(51) König, D., Jiang, C.W., Conibeer, G., Takeda, Y., Ito, T. and Motohiro, T., *Proc. 21st European Photovoltaic Solar Energy Conference* (2006), pp.366-369.
(52) Yagi, S. and Okada, Y., *Proc. 35th IEEE Photovoltaic Specialists Conference* (2010), pp.1213-1216.
(53) Takeda, Y., Motohiro, T., König, D., Aliberti, P., Feng, Y., Shrestha, S. K. and Conibeer, G., *Appl. Phys. Express*, Vol.3 (2010), 104301.
(54) Takeda, Y., Ito, T., Motohiro, T., König, D., Shrestha, S. and Conibeer, G., *J. Appl. Phys.*, Vol.105 (2009), 074905.
(55) Humphrey, T. E., Newbury, R., Taylor, R. P. and Linke, H., *Phys. Rev. Lett.*, Vol.89 (2002), 116801.
(56) Markvart, T., *Phys. Stat. Sol. (a)*, Vol.205 (2008), pp.2752-2756.
(57) Hirst, L. C., Ekins-Daukes, N. J., *Prog. Photovolt.: Res. Appl.*, Vol.19 (2011), pp.286-293.
(58) Takeda, Y., Ito, T., Suzuki, R., Motohiro, T., Shrestha, S. and Conibeer, G., *Solar Energy Mater. Solar Cells*, Vol.93 (2009), pp.797-802.
(59) Ryan, J. F., Taylor, R. A., Turberfield, A. J. and Maciel, A., *Phys. Rev. Lett.*, Vol.53 (1984), pp.1841-1844.
(60) Rosenwaks, Y., Hanna, M. C., Levi, D. H., Szmyd, D. M., Ahrenkiel, R. K. and Nozik, A. J., *Phys. Rev. B*, Vol.48 (1993), pp.14675-14678.
(61) Luque, A. and Martí, A., *Solar Energy Mater. Solar Cells*, Vol.94 (2010), pp.287-296.
(62) Snoke, D. W., *Phys. Rev. B*, Vol.50 (1994), pp.11583-11591.
(63) Davis, J. H, *The Physics of Low-dimensional Semiconductors* (1998), Chap. 5., Cambridge Univ. Press.
(64) Veetill, B. P., Patterson, T., König, D., Conibeer, G. and Green, M. A., *Europhys. Lett.*, Vol.96 (2011), 57006.
(65) Conibeer, G., Ekins-Daukes, N., Guillemoles, J.-F., König, D., Cho, E.-C., Jiang, C.-W., Shrestha, S. and Green, M., *Solar Energy Mater. Solar Cells*, Vol.93 (2009), pp.713-719.
(66) Bryllert, T., Borgstrom, M., Sass, T., Gustafson, B., Landin, L., Wernersson, L.-E., Seifert, W. and Samuelson, L., *Appl. Phys. Lett.*, Vol.80 (2002), pp.2681-2683.
(67) Takeda, Y. and Motohiro, T., *Solar Energy Mater. Solar Cells*, Vol.95 (2011), pp.2638-2644.
(68) Le Bris, A. and Guillemoles, J.-F., *Appl. Phys. Lett.*, Vol.97 (2010), 113506.
(69) Aliberti, P., Feng, Y., Shrestha, S. K., Green, M. A., Conibeer, G., Tu, L. W., Tseng, P. H. and Clady, R., *Appl. Phys. Lett.*, Vol.99 (2011), 223507.
(70) Feng, Y., Aliberti, P., Veettil, B. P., Patterson, R., Shrestha, S., Green, M. A. and Conibeer, G., *Appl. Phys. Lett.*, Vol.100 (2012), 053502.
(71) Le Bris, A., Lombez, L., Laribi, S., Boissier, G., Christold, P. and Guillemoles, J.-F., *Energy Environ. Sci.*, Vol.5 (2012), pp.6225-6232.
(72) König, D., Casalenuovo, K., Takeda, Y., Conibeer, G., Guillemoles, J.-F., Patterson, R., Huang, L. M. and Green, M. A., *Physica E*, Vol.42 (2010), pp.2862-2866.
(73) Patterson, R., Kirkengen, M., Puthen-Veettil, B., König, D., Green, M. A. and Conibeer, G., *Solar Energy Mater. Solar Cells*, Vol.94 (2010), pp.1931-1935.
(74) König, D., Takeda, Y. and Puthen-Veettil, B., "Technology-compatible Hot Carrier Solar Cell with Energy Selective Hot Carrier Absorber and Carrier-selective Contacts", *Appl. Phys. Lett*., in press.
(75) Farrell, D. J., Takeda, Y., Nishikawa, K., Nagashima, T., Motohiro, T. and Ekins-Daukes, N. J., *Appl. Phys. Lett.*, Vol.99 (2011), 111102.
(76) Takeda, Y. and Motohiro, T., "Hot-carrier Extraction from Intermediate-band Absorbers through Quantum-well Energy-selective Contacts", *Jpn. J. Appl. Phys*., in press.
(77) Takeda, Y. and Motohiro, T., "Intermediate-band-assisted Hot-carrier Solar Cells Using Indirect-bandgap Absorbers", *Prog. Photovolt.: Res. Appl.*, in press.

Figs. 7 and 9-11
Reprinted from J. Appl. Phys., Vol.105 (2009), 074905, Takeda, Y., Ito, T., Motohiro, T., König, D., Shrestha, S. and Conibeer, G., Hot Carrier Solar Cells Operating under Practical Conditions, © 2009 AIP, with permission from American Institute of Physics.

Yasuhiko Takeda
Research Fields:
- Solar Cells
- Optical and Transport Properties of Nanostructured Materials

Academic Degree: Dr.Eng.
Academic Society:
- The Japan Society of Applied Physics

Awards:
- R&D 100 Award, 2000
- Best Poster Award of Renewable Energy, 2006
- The 20 Highest Scored Abstracts of the 27th European Photovoltaic Solar Energy Conference, 2012

Tomoyoshi Motohiro
Research Fields:
- Solar Energy Utilization and Laser Fusion
- Thin Films and Surface Science

Academic Degree: Dr.Eng.
Academic Societies:
- The Surface Science Society of Japan
- The Japan Society of Applied Physics
- Materials Research Society
- Society of Automotive Engineers of Japan
- Society of Science on Form, Japan
- Optical Society of Japan

Awards:
- R&D 100 Award, 2000
- Best Poster Award of Renewable Energy, 2006
- Poster Award of the 109th Symposium of Catalysis Society of Japan, 2012
- The 20 Highest Scored Abstracts of the 27th European Photovoltaic Solar Energy Conference, 2012

